Hepatitis C Virus IRES RNA–Induced Changes in the Conformation of the 40*S* Ribosomal Subunit

Christian M. T. Spahn,[1,2]* Jeffrey S. Kieft,[3]*
Robert A. Grassucci,[1,2] Pawel A. Penczek,[2]† Kaihong Zhou,[3]
Jennifer A. Doudna,[3]‡ Joachim Frank[1,2,4]†

Initiation of protein synthesis in eukaryotes requires recruitment of the 40*S* ribosomal subunit to the messenger RNA (mRNA). In most cases, this depends on recognition of a modified nucleotide cap on the 5′ end of the mRNA. However, an alternate pathway uses a structured RNA element in the 5′ untranslated region of the messenger or viral RNA called an internal ribosomal entry site (IRES). Here, we present a cryo-electron microscopy map of the hepatitis C virus (HCV) IRES bound to the 40*S* ribosomal subunit at about 20 Å resolution. IRES binding induces a pronounced conformational change in the 40*S* subunit and closes the mRNA binding cleft, suggesting a mechanism for IRES-mediated positioning of mRNA in the ribosomal decoding center.

Initiation of protein synthesis in eukaryotes requires the ordered assembly of ribosomal preinitiation complexes. The ribosome dynamics that accompany this process are not understood, although recent progress in determining the structure of ribosomes and functional ribosomal complexes by x-ray crystallography (*1*–*4*) and cryo–electron microscopy (cryo-EM) (*5*–*8*) has revealed changes and variations in ribosome structure that occur during the elongation stage of protein synthesis in prokaryotes. Canonical eukaryotic cap-dependent translation initiation involves a complex pathway during which a large number of factors interact with the ribosome and one another (*9*) (Fig. 1A). An alternate pathway, called internal initiation of translation, is a cap-independent, end-independent mechanism of recruiting, positioning, and activating the eukaryotic protein synthesis machinery, driven by structured RNA sequences called internal ribosome entry sites (IRESs) located in the mRNA 5′ untranslated region (UTR) (*10*) (Fig. 1A). These sequences were first identified in many viral RNAs, but the number of known eukaryotic mRNAs that use an IRES mechanism is growing.

In hepatitis C virus (HCV), a human pathogen and world-wide health threat, the minimal sequence and secondary structure requirements of HCV IRES–driven translation have been defined, the presence and architecture of an IRES RNA tertiary fold has been described, and the identity and binding sites of necessary cofactors have been determined (*11*) (Fig. 1B). The HCV IRES forms an extended structure that binds the 40*S* ribosomal subunit and eukaryotic initiation factor 3 (eIF3) through multiple intermolecular contacts, resulting in precise placement of the start codon in the ribosome decoding site (*12*–*14*). To address the molecular mechanism by which the HCV IRES RNA recruits the eukaryotic translation machinery, we have generated three-dimensional reconstructions of HCV IRES RNA bound to the rabbit 40*S* ribosomal subunit. Reconstructions at 20 Å resolution produced by cryo-EM in combination with the single-particle approach (*15*) reveal that HCV IRES RNA actively manipulates the translational machinery through extensive and specific intermolecular interactions.

The structure of the rabbit 40*S* ribosomal subunit obtained as a control displays the classical division into body, head, and platform domains (Fig. 2, A to C). It represents the first reconstruction of a eukaryotic ribosomal subunit from zero-tilt images and has a greatly improved resolution compared with a previous random-conical tilt reconstruction (*16*). Although the resolution is lower than currently obtained with 70*S* (*5*, *17*) or 80*S* ribosomes, the overall structure of the rabbit 40*S* subunit compares well with the 40*S* part of a reconstruction of the yeast 80*S* ribosome (*18*). Density attributable to the HCV IRES RNA appears directly in the map of the IRES RNA–40*S* subunit complex and can be seen in the difference map between the complex and the vacant 40*S* subunit as an extended structure (Fig. 2, D and F). The cross-sectional diameter and overall shape of the IRES density is consistent with A-form helices extending from regions of denser packing or more convoluted structure (Fig. 1, C and D). Previous small-angle x-ray scattering experiments suggested that the unbound, folded HCV IRES RNA maintained some conformational flexibility (*14*). The new results show that the IRES assumes a single conformation when bound to the 40*S* subunit.

The IRES RNA is bound to the solvent side of the 40*S* subunit in a position that is consistent with the proposed path of the mRNA through the subunit (*19*). The 5′ end of the single-stranded coding RNA is expected to exit the ribosome through a channel that is built by the neck, the head, and the platform domains (*20*). Two segments of the IRES RNA density extend from this exit channel, one toward the head, and the other to the back of the platform (*21*). There are no contacts with the intersubunit face of the 40*S* subunit, consistent with the observation that 80*S* ribosomes can be assembled without removal of the HCV IRES RNA (*12*).

To assign the HCV IRES density to RNA structural domains, we used a truncated HCV IRES construct in which domain II is deleted; this mutant binds the 40*S* subunit with nearly wild-type affinity (Fig. 1B) (*13*). IRES RNA density missing from the structure of this truncated IRES–40*S* subunit complex (Fig. 2, G to I) unambiguously identifies domain II (Fig. 2, D to F, and Fig. 3). From this assignment, we deduce that the globular density that contacts the back of the platform contains domain IIId/e/f stem-loops and junctions, whereas the remaining density extending away from the 40*S* subunit surface corresponds to IIIb, IIIa, and IIIc (Fig. 3). Domain IIIb is not involved in 40*S* subunit binding, but is known to make specific contacts with eIF3 (*13*, *22*). An earlier reconstruction of eIF3 bound to the 40*S* subunit (*23*) shows that this factor interacts with the 40*S* subunit in the region where domain IIIb of the HCV IRES RNA is seen to extend from the ribosome surface (Fig. 3). Thus, even in the absence of eIF3, the IRES RNA domain IIIb is properly positioned to bind this factor.

HCV IRES domain II is a particularly interesting feature of the bound RNA structure. This domain loops away from the 40*S* subunit surface, making contact only at the apical half of the domain. The sequence of

[1]Howard Hughes Medical Institute, Health Research Inc. at the [2]Wadsworth Center, Empire State Plaza, Albany, New York 12201–0509, USA. [3]Department of Molecular Biophysics and Biochemistry and Howard Hughes Medical Institute, Yale University, New Haven, CT 06520–8114, USA. [4]Department of Biomedical Sciences, State University of New York at Albany, Albany, NY 12222, USA.

*These authors contributed equally to this work.
†Present address: Department of Biochemistry, University of Texas, Health Science Center, Houston, TX 77030, USA.
‡To whom correspondence should be addressed. E-mail: doudna@csb.yale.edu and joachim@wadsworth.org

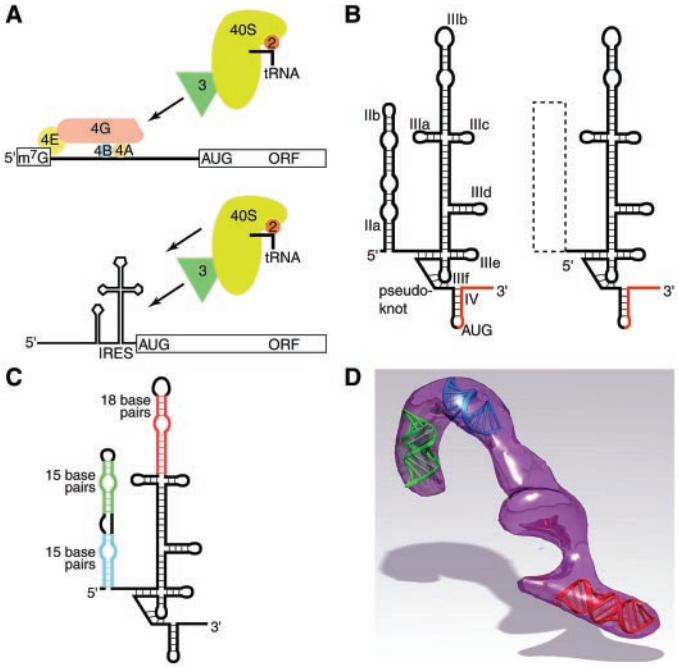

Fig. 1. Hepatitis C virus ribosome recruitment strategy, IRES secondary structure, and modeling of example A-form RNA helices into HCV IRES density. (**A**) Comparison of canonical eukaryotic cap-dependent translation initiation (top) and the internal initiation mechanism used by hepatitis C virus (bottom). Cap-dependent translation requires recognition of a modified nucleotide at the 5′ terminus of the mRNA by the eIF4F complex, which includes eIF-4G, eIF-4E, eIF-4B, and eIF-4A. The 43*S* particle (40*S* subunit/eIF3/Met-tRNA/eIF2/GTP) binds to the mRNA/eIF4F complex primarily through interactions between eIF3 and eIF4G. In contrast, HCV IRES–driven translation initiation occurs through direct, specific recognition of the 40*S* subunit and eIF3 by the IRES RNA tertiary structure, eliminating the need for the cap-structure and cap-binding factors. (**B**) Schematic secondary structures of the HCV IRES RNA constructs used in this study. The full-length construct (left) consists of nucleotides 40 to 372 of HCV IRES genotype 1b, and is fully active in initiation translation. Thirty nucleotides of the coding RNA are included in this construct and are shown in red. The deletion mutant (right) contains nucleotides 119 to 372, has diminished translation initiation activity, but binds the 40*S* subunit with wild-type activity. (**C**) Locations within the secondary structure and sizes of RNA helices that were fit into the HCV IRES density (purple). For the purpose of modeling, structure throughout internal loops was approximated by continuous base stacking into helices of 15 base pairs (cyan), 15 base pairs (green), and 18 base pairs (red). (**D**) Placement of helices into a surface representing the 40*S* bound IRES RNA density reveals a good fit both in terms of helical diameter and lengths. A-form RNA helices shown in (D) were generated in NAMOT2 and SPOCK; images were created with RIBBONS (*47*) and POVRAY.

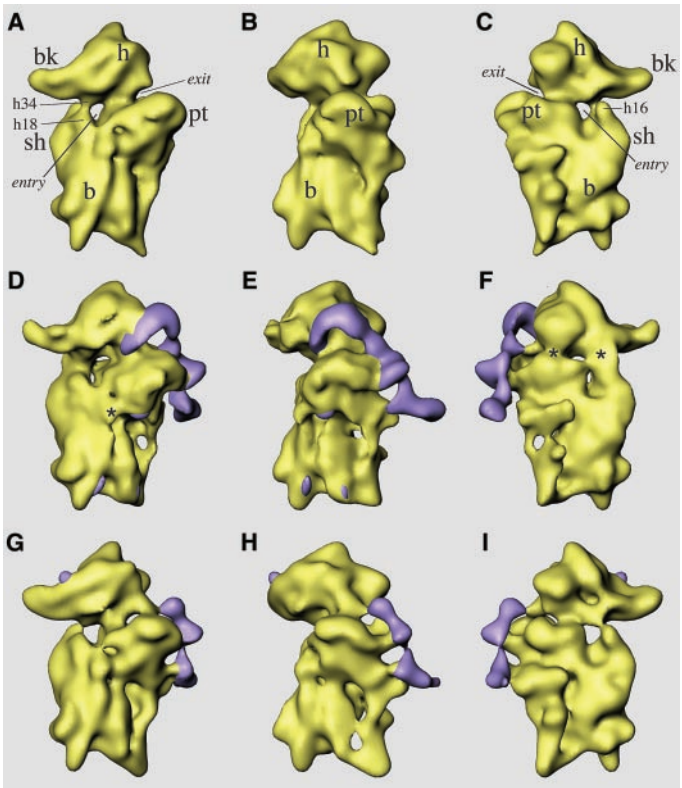

Fig. 2. Surface representation of the vacant 40*S* ribosomal subunit from rabbit reticulocytes (**A** to **C**), the 40*S* subunit in complex with the HCV IRES RNA (**D** to **F**), and the 40*S* subunit in complex with the truncated HCV IRES RNA, where domain II has been deleted (**G** to **I**). The cryo-EM maps are shown in yellow. The difference maps corresponding to the full-length HCV IRES RNA (D to F) or the deletion mutant (G to I) are superposed and shown in purple. The views are from the 60*S* side of the 40*S* subunit (A, D, and G), the platform side (B, E, and H), and the solvent side (C, F, and I). Some landmarks of the 40*S* subunit are indicated: b, body; bk, beak; h, head; pt, platform; sh, shoulder. "Entry" and "exit" label the proposed entry and exit path, respectively, of the mRNA (*26*, *31*). h16, h18, and h34 indicate the positions of helices 16, 18, and 34, respectively, of the 18*S* rRNA as identified by comparison with a cryo-EM map of the 80*S* ribosome from yeast (*28*). Some conformational changes in the IRES RNA–40*S* subunit complex referred to in the text are indicated with asterisks (D and F).

the IIb terminal loop and adjacent helix are found in other viral IRESs, suggesting this contact may be an important determinant not only of HCV IRES function but also of other, similar, viral IRESs (*24*). The contact between domain II and the 40*S* subunit occurs in a region of the head and the edge of the platform. Thus, domain II partially overlaps with the E site, the binding site occupied by deacylated tRNA before it exits the ribosome (*4*, *25*). This contact is the only HCV IRES–40*S* subunit interaction that approaches the active site of the ribosome, and it lies near the 60*S* subunit binding face. The binding of domain II closes the mRNA binding cleft from the 60*S* side, restricting the movement of coding RNA within the cleft. Single-stranded RNA is not likely to be resolved at the present resolution and is difficult to detect even in higher-resolution cryo-EM maps of the 70*S* ribosome (*5*, *26*). However, a small extension of density pointing into the mRNA binding cleft, which grows when the contour level of the difference map is lowered (not shown), might be part of the single-stranded coding RNA. This observation suggests that the domain II terminal loop may contact the single-stranded coding part of the viral RNA. Although the presence of noise in the difference map at such low contour level (not shown) prevents a definite conclusion, it is tempting to speculate that part of the function of domain II is to place the single-stranded coding part of the RNA into the decoding center.

Binding of the HCV IRES RNA to the 40*S* subunit induces a conformational change in the 40*S* subunit, the first reported example of a structured viral RNA that binds to, and actively manipulates, the structure of a cellular machine. The structural change involves a change in the orientation of the head relative to the body, which can be recognized in a different position of the beak part of the head domain in the IRES RNA–40*S* subunit complex (Fig. 2, D to F) compared with the vacant 40*S* subunit (Fig. 2, A to C) (*27*). The platform domain also changes shape, and several more localized changes can be observed (marked with asterisks in D and F of

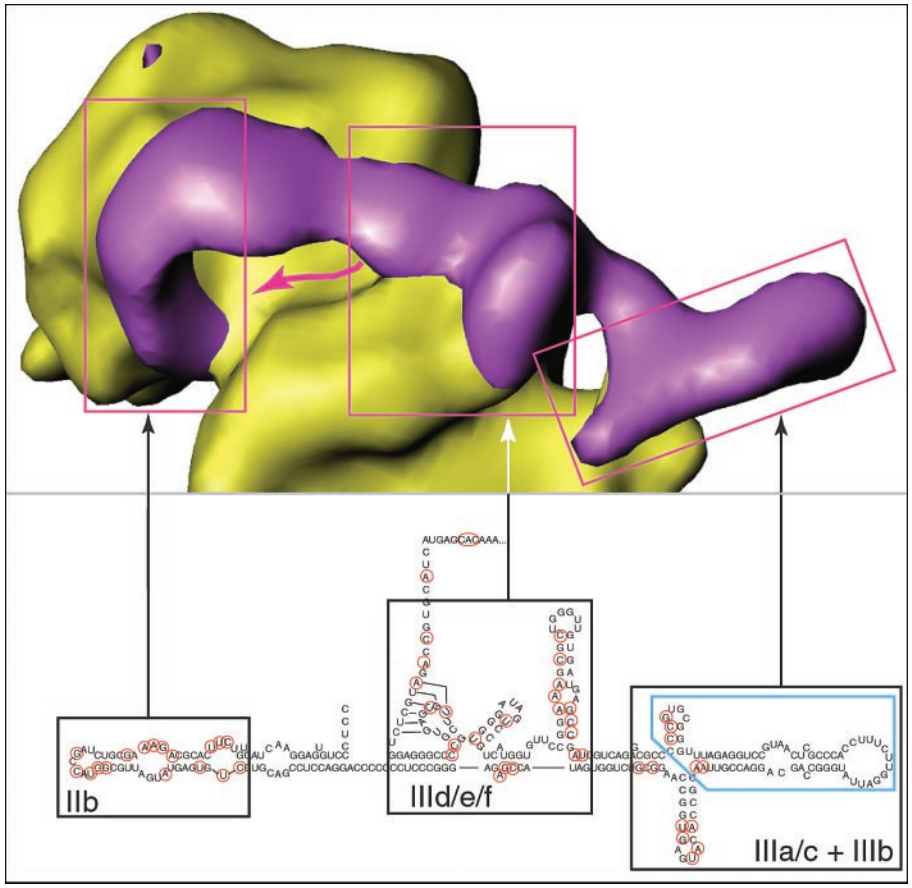

Fig. 3. Correlation of chemical probing data with the cryo-EM structure of the HCV IRES RNA–40*S* subunit complex, and assignment of IRES RNA structural domains within the structure. The three IRES RNA tertiary structural elements that were previously identified by chemical and enzymatic probing are boxed within the secondary structure. The secondary structure is depicted in a manner that better reflects its organization on the 40*S* subunit surface. Arrows link the tertiary structure domains to the corresponding elements within the IRES RNA cryo-EM structure. The strategy used to assign density to these domains is described in the text. Within the secondary structure, nucleotides that were previously reported to be inaccessible to solvent upon 40*S* subunit binding are circled in red (*13*). The location of the eIF3 binding site on domain IIIb and IIIa is boxed in blue; this domain extends away from the 40*S* subunit surface. The protection pattern sites agree with the locations of intermolecular contacts observed in the cryo-EM representations. A magenta arrow pointing to the 3′ end delineates the probable location of the coding RNA in the mRNA binding groove.

Fig. 2). The rotation of the head and a slight rearrangement of the shoulder region lead to a broad fusion of the shoulder with the underside of the head. In a detailed analysis of a higher-resolution cryo-EM map of the yeast 80*S* ribosome, the rod-like structure that extends from the top of the 40*S* subunit shoulder toward the solvent side and fuses with the head upon HCV IRES binding (Fig. 2F, asterisk on right) was identified as helix 16 of 18*S* ribosomal RNA (rRNA) (*28*). Thus, the position of helix 16 differs from that in prokaryotes, where it is folded toward helix 18 of 16*S* rRNA (the 530 pseudoknot structure). Helix 18, in turn, is involved in a noncovalent junction with helix 34 of the head domain (*2*, *3*, *29*, *30*). This junction or latch has been proposed to be part of the mRNA entry channel and to clamp around the incoming strand of the mRNA (*31*). The fusing of the helix 16 density with the underside of the head effectively alters the shape of the entry site of the mRNA, apparently clamping down on the solvent side (compare C and F of Fig. 2). However, the latch between helices 18 and 34, which can be observed in the vacant 40*S* subunit, is opened, possibly helping the 3′ end of the coding RNA to thread into the mRNA entry channel. In this respect, the HCV IRES might work analogously to the clamp-loading machinery in DNA replication (*32*).

The conformational change induced by the binding of full-length HCV IRES RNA is not observed when the domain II deletion mutant is bound to the 40*S* subunit and, therefore, must be a consequence of domain II's interaction at or near the E site (Fig. 2, G to I). Although domain II does not contribute to IRES affinity for the 40*S* subunit, and isolated domain II does not bind to the 40*S* subunit (*33*), removal of domain II is deleterious to the ability of the IRES to initiate translation (*34*).

The HCV IRES RNA-induced structural change in the 40*S* ribosomal subunit could have significance in activating, or promoting initiation of, translation without the help of certain canonical initiation factors. Domain II may hold the coding RNA in position in the decoding site until the rest of the translation machinery has assembled and elongation has begun (*35*). In addition, HCV IRES binding could capture a 40*S* subunit conformation that is favorable for continued preinitiation complex assembly (*36*).

Previous models of HCV IRES action have focused on the binding of the 40*S* subunit to an IRES RNA scaffold in a mechanism reminiscent of the role of the Shine-Dalgarno sequence in prokaryotes. Our findings call for an expansion of these models such that IRES RNA actively manipulates the host cell's translation machinery to orchestrate the assembly of the preinitiation complex. This raises the interesting questions of whether other viral or eukaryotic IRES RNAs use similar mechanisms to alter the conformation of the translational machinery, and whether these observed structural changes may be common and required steps in cap- and end-dependent pathways of eukaryotic translation initiation. A deeper understanding of the conformational changes and intermolecular signals that occur in IRES-driven translation initiation may offer insights into the events that are common features of all types of translation initiation in eukaryotes.

References and Notes

1. N. Ban, P. Nissen, J. Hansen, P. B. Moore, T. A. Steitz, *Science* **289**, 905 (2000).
2. B. T. Wimberly *et al.*, *Nature* **407**, 327 (2000).
3. F. Schlunzen *et al.*, *Cell* **102**, 615 (2000).
4. J. H. Cate, M. M. Yusupov, G. Zh. Yusupova, T. N. Earnest, H. F. Noller, *Science* **285**, 2095 (1999).
5. I. S. Gabashvili *et al.*, *Cell* **100**, 537 (2000).
6. J. Frank, R. K. Agrawal, *Nature* **406**, 318 (2000).
7. H. Stark *et al.*, *Nature* **389**, 403 (1997).
8. R. K. Agrawal, J. Frank, *Curr. Opin. Struct. Biol.* **9**, 215 (1999).
9. W. C. Merrick, J. W. B. Hershey, *Translational Control*, J. W. B. Hershey, M. B. Mathews, N. Sonenberg, Eds. (Cold Spring Harbor Laboratory Press, Cold Spring Harbor, NY, 1996), p. 31.
10. R. J. Jackson, *Translational Control*, J. W. B. Hershey, M. B. Mathews, N. Sonenberg, Eds. (Cold Spring Harbor Laboratory Press, Cold Spring Harbor, NY, 1996), p. 71.
11. R. C. Rijnbrand, S. M. Lemon, *Curr. Top. Microbiol. Immunol.* **242**, 85 (2000).
12. T. V. Pestova, I. N. Shatsky, S. P. Fletcher, R. J. Jackson, C. U. T. Hellen, *Genes Dev.* **12**, 67 (1998).
13. J. S. Kieft, K. Zhou, R. Jubin, J. A. Doudna, *RNA* **7**, 194 (2001).
14. J. S. Kieft *et al.*, *J. Mol. Biol.* **292**, 513 (1999).
15. The 40*S* subunits from rabbit reticulocytes and HCV IRES RNA were prepared as described previously (*13*). To generate IRES RNA–40*S* subunit complexes, RNA was annealed by heating to 75°C for 1 min, then cooled to room temperature. RNA was then added to a tube containing folding/binding buffer [20 mM

tris-HCl, 100 mM potassium acetate, 200 mM KCl, 2.5 mM $MgCl_2$, 1 mM dithiothreitol (DTT)], followed by addition of stoichiometric amounts of 40*S* subunit and incubation at 37°C for 15 min. The final complex concentration was about 500 nM. The samples were snap-frozen with liquid nitrogen and stored at −80°C until use.

Samples of 40*S* subunits (final concentration about 50 nM) were applied to cryo-EM grids and shock-frozen in liquid ethane (*37*, *38*). Micrographs were recorded under low-dose conditions in a defocus range between 1.7 μm and 5.7 μm on a Philips F20 (FEI/Philips) at a magnification of 50.000 ± 2%. From the micrographs, 69 were selected for the vacant 40*S* subunit, 74 for the IRES-40*S* complex, and 61 for the IRESΔdII-40*S* complex. The micrographs were scanned on a Highscan drum scanner (Eurocore/Saint-Denis, France) with a resolution of 1069 dpi corresponding to a pixel size of 4.78 Å on the object scale. The data were analyzed using the SPIDER system (*39*). After automated particle preselection, manual verification, and selection by cross-correlation, 18,801 particles were chosen for the vacant 40*S* subunit, 20,939 particles for the IRES-40*S* complex, and 13,613 particles for the IRESΔdII-40*S* complex. The data sets were subdivided each into 16 to 23 defocus groups, and a refined, three-dimensional reconstruction that was corrected for the contrast transfer function was calculated for each of the 40*S* samples (*40*). The final resolution was estimated by the Fourier shell correlation with a cutoff value of 0.5. It is 22.7 Å for the vacant 40*S* subunit, 19.8 Å for the IRES-40*S* complex, and 21.9 Å for the IRESΔdII-40*S* complex. According to the more lenient (*17*) 3σ criterion (*41*), the resolution values would be 15.9 Å, 14.5 Å, and 15.4 Å, respectively.

16. S. Srivastava, A. Verschoor, M. Radermacher, R. Grassucci, J. Frank, *J. Mol. Biol.* **245**, 461 (1995).
17. A. Malhotra *et al.*, *J. Mol. Biol.* **280**, 103 (1998).
18. M. G. Gomez-Lorenzo *et al.*, *EMBO J.* **19**, 2710 (2000).
19. J. Frank *et al.*, *Nature* **376**, 441 (1995).
20. J. Frank *et al.*, *Biochem. Cell Biol.* **73**, 757 (1995).
21. To our knowledge, the ribosomal region at the back of the platform has not been previously implicated in molecular recognition of a ribosomal ligand. As does the protein conducting channel Sec61 (translocon) (*42*, *43*), the HCV IRES recognizes the evolutionarily more divergent outer surfaces of the ribosome. Thus, the surfaces available for specific molecular recognition extend beyond the highly conserved binding sites for tRNAs and elongation factors. The fact that the HCV IRES binds to the more variable regions of the 40*S* subunit surface may explain its ability to distinguish the 40*S* subunit of rabbit from that of wheat germ (*12*).
22. D. V. Sizova, V. G. Kolupaeva, T. V. Pestova, I. N. Shatsky, C. U. Hellen, *J. Virol.* **72**, 4775 (1998).
23. S. Srivastava, A. Verschoor, J. Frank, *J. Mol. Biol.* **226**, 301 (1992).
24. M. Honda, M. R. Beard, L. H. Ping, S. M. Lemon, *J. Virol.* **73**, 1165 (1999).
25. R. K. Agrawal *et al.*, *J. Cell Biol.* **150**, 447 (2000).
26. J. Frank *et al.*, *The Ribosome*: *Structure Function Antibiotics and Cellular Interactions*, R. A. Garrett *et al.*, Eds. (ASM Press, Washington, DC, 2000), p. 45.
27. An animated sequence showing the conformational change is available as supplementary material on *Science* Online at www.sciencemag.org/cgi/content/full/291/5510/1959/DC1.
28. C. M. Spahn, R. Beckmann, G. Blobel, J. Frank, unpublished observations.
29. C. M. T. Spahn, P. Penczek, A. Leith, J. Frank, *Structure Fold. Des.* **8**, 937 (2000).
30. A. P. Carter *et al.*, *Nature* **407**, 340 (2000).
31. K. R. Lata *et al.*, *J. Mol. Biol.* **262**, 43 (1996).
32. S. Waga, B. Stillman, *Annu. Rev. Biochem.* **67**, 721 (1998).
33. J. S. Kieft, K. Zhou, J. A. Doudna, unpublished observations.
34. Moreover, deletion of domain II strongly reduces an ultraviolet radiation-induced cross-link between the IRES RNA and ribosomal protein S9 (the homolog of bacterial protein S4) (*44*). Electron microscopy of antibody-labeled 40*S* subunits located S9 at the back of the shoulder, below helix 16, near the mRNA binding cleft entry site (*45*), in agreement with the placement of bacterial S4 within the 30*S* subunit (*2*, *3*, *46*). This position is quite far away from the structured part of the HCV IRES RNA in our density map, suggesting that the IRES RNA-S9 cross-link occurs to the coding part of the IRES RNA just 3′ of the start codon (*12*). Thus, the domain II–induced changes in the ribosome structure around the coding RNA, as well as the direct restriction of movement of the single-stranded coding part of the RNA by the terminal loop of domain II (see above), may explain the differing efficiencies of the S9-RNA cross-link between IRES RNA with and without domain II.
35. This would be consistent with toe-printing experiments that show a decrease in the intensity of the stop associated with mRNA bound in the cleft when domain II is removed (*44*). Removal of domain II also causes a slight change in the position of IRES RNA domain IIIb relative to the surface of the 40*S* subunit, although binding data show that the overall IRES RNA affinity for the 40*S* subunit remains unchanged and that there are no changes in ribosome structure in this region. The significance of this observation is presently not clear.
36. It is difficult to imagine domain II remaining in place during elongation, as this would restrict both coding RNA and ribosome movement; some mechanism must exist to release this contact. Perhaps once elongation has begun, tRNA moving into the E site during the translocation step might displace domain II, effectively releasing the ribosome from its IRES-induced conformation, opening up the entry site for incoming coding RNA, and allowing unrestricted ribosome movement during elongation. Alternatively, subunit association could move the 40*S* subunit out of its IRES-induced conformation, thus ejecting domain II from its contact point.
37. T. Wagenknecht, R. Grassucci, J. Frank, *J. Mol. Biol.* **199**, 137 (1988).
38. J. Dubochet *et al.*, *Q. Rev. Biophys.* **21**, 129 (1988).
39. J. Frank *et al.*, *J. Struct. Biol.* **116**, 190 (1996).
40. J. Frank, P. Penczek, R. K. Agrawal, R. A. Grassucci, A. B. Heagle, *Methods Enzymol.* **317**, 276 (1999).
41. E. V. Orlova *et al.*, *J. Mol. Biol.* **271**, 417 (1997).
42. R. Beckmann *et al.*, *Science* **278**, 2123 (1997).
43. J. F. Ménétret *et al.*, *Mol. Cell* **6**, 1219 (2000).
44. V. G. Kolupaeva, T. V. Pestova, C. U. Hellen, *J. Virol.* **74**, 6242 (2000).
45. G. Lutsch, H. Bielka, G. Enzmann, F. Noll, *Biomed. Biochim. Acta* **42**, 705 (1983).
46. W. M. Clemons Jr. *et al.*, *Nature* **400**, 833 (1999).
47. M. Carson, *J. Appl. Crystallogr.* **24**, 103 (1991).
48. This work was funded, in part, by grants from NIH (R37 GM29169 to J.F. and GM60635 to P.A.P) and NSF (DBI 9871347 to J.F.). We thank Y. Chen for assistance with the illustrations and R. T. Batey, P. Adams, and P. Masters for critically reading the manuscript.

18 December 2000; accepted 25 January 2001

A Proteolytic Transmembrane Signaling Pathway and Resistance to β-Lactams in Staphylococci

H. Z. Zhang, C. J. Hackbarth, K. M. Chansky, H. F. Chambers*

β-Lactamase and penicillin-binding protein 2a mediate staphylococcal resistance to β-lactam antibiotics, which are otherwise highly clinically effective. Production of these inducible proteins is regulated by a signal-transducing integral membrane protein and a transcriptional repressor. The signal transducer is a fusion protein with penicillin-binding and zinc metalloprotease domains. The signal for protein expression is transmitted by site-specific proteolytic cleavage of both the transducer, which autoactivates, and the repressor, which is inactivated, unblocking gene transcription. Compounds that disrupt this regulatory pathway could restore the activity of β-lactam antibiotics against drug-resistant strains of staphylococci.

β-Lactam antibiotics are the most effective drugs for the treatment of staphylococcal infections, yet they often cannot be used because many strains are resistant. Resistance is due to production of either β-lactamase or an extra penicillin-binding protein, PBP 2a (*1*, *2*). β-Lactamase, encoded by *blaZ*, inactivates penicillin by hydrolysis of its β-lactam ring. PBP 2a, encoded by the chromosomal gene *mecA*, in methicillin-resistant strains of staphylococci, confers resistance not only to penicillin, but also to all β-lactam antibiotics. PBP 2a, which is probably a transpeptidase (*3*), can substitute for other PBPs but, because of its low affinity for binding β-lactams, is unbound at clinically relevant concentrations of antibiotic, allowing cell wall synthesis to continue (*4*). Although β-lactamase and PBP 2a are genetically and biochemically distinct, both are regulated by similar sensor-transducer and repressor proteins. Their regulatory proteins are homologs of each other and of those controlling expression of inducible β-lactamase in *Bacillus licheniformis* (*5*–*7*). In staphylococci, the

Division of Infectious Diseases, San Francisco General Hospital, Department of Medicine, University of California at San Francisco, 1001 Potrero Avenue, San Francisco, CA 94110, USA.

*To whom correspondence should be addressed. E-mail: chipc@itsa.ucsf.edu